An In Situ Al K-Edge XAS Investigation of the Local Environment of H^+- and Cu^+-Exchanged USY and ZSM-5 Zeolites

Ian J. Drake,[†] Yihua Zhang,[†] Mary K. Gilles,[‡] C. N. Teris Liu,[†,§] Ponnusamy Nachimuthu,[||,⊥] Rupert C. C. Perera,[⊥] Hisanobu Wakita,[#] and Alexis T. Bell*[†,‡,§]

Department of Chemical Engineering, University of California, Berkeley, California 94720-1462, Chemical Sciences Division, Lawrence Berkeley National Laboratory, 1 Cyclotron Road, Berkeley, California 94720, Department of Chemistry, University of California, Berkeley, California 94720, Department of Chemistry, University of Nevada, Las Vegas, Nevada 89154, Lawrence Berkeley National Laboratory, Berkeley, California 94720, and Advanced Materials Institute and Department of Chemistry, Faculty of Science, Fukuoka University, Nanakuma, Jonan-ku, Fukuoka 814-0180, Japan

Received: September 2, 2005

Aluminum coordination in the framework of USY and ZSM-5 zeolites containing charge-compensating cations (NH_4^+, H^+, or Cu^+) was investigated by Al K-edge EXAFS and XANES. This work was performed using a newly developed in-situ cell designed especially for acquiring soft X-ray absorption data. Both tetrahedrally and octahedrally coordinated Al were observed for hydrated H−USY and H−ZSM-5, in good agreement with ^{27}Al NMR analyses. Upon dehydration, water desorbed from the zeolite, and octahedrally coordinated Al was converted progressively to tetrahedrally coordinated Al. These observations confirmed the hypothesis that the interaction of water with Brønsted acid protons can lead to octahedral coordination of Al without loss of Al from the zeolite lattice. When H^+ is replaced with NH_4^+ or Cu^+, charge compensating species that absorb less water, less octahedrally coordinated Al was observed. Analysis of Al K-edge EXAFS data indicates that the Al−O bond distance for tetrahedrally coordinated Al in dehydrated USY and ZSM-5 is 1.67 Å. Simulation of $k^3\chi(k)$ for Cu^+ exchanged ZSM-5 leads to an estimated distance between Cu^+ and framework Al atoms of 2.79 Å.

Introduction

Zeolites are crystalline, microporous aluminosilicates, used extensively as catalysts for petroleum processing, chemical synthesis, and abatement of gaseous pollutants.[1−4] The zeolite framework consists of corner-linked SiO_4^{4-} and AlO_4^{5-} tetrahedra. Because of the difference in Si and Al valences, the presence of tetrahedrally coordinated Al in the zeolite framework creates an anionic site that must be charge compensated with a cation. In the acidic form of the zeolite, this cation is a proton. Exchanging the proton for a metal cation leads to the M form of the zeolite.[1,5] Since the active center in zeolite catalysts is either a Brønsted acid or a metal cation, it is important to understand the factors affecting the activity of this site. Previous research has shown that the acidity of the H^+ form of a zeolite is affected by the local geometry of the site, including factors such as the Al−O bond distance and the Al−O−Si angle.[6,7] By contrast, little is known about the effects of site geometry on the properties of sites involving metal cations. However, geometry is expected to be important since it affects the orbital overlap between the framework O atoms in the vicinity of the exchange site and the coordinated metal cation.[8,9] In light of these considerations, there is a need to determine the local coordination and geometry of Al atoms in the framework of zeolites and to understand how they change when the zeolite is exposed to a variety of chemical environments at both ambient and elevated temperatures.

Characterization of the Al local environment in zeolites has proven to be challenging. Due to the similarity in the scattering properties of Al and Si atoms, X-ray and neutron diffraction do not differentiate between Al and Si in zeolites, with the exception when the Si/Al ratio is one.[10] ^{27}Al MAS NMR has been the most commonly used technique for characterizing the local coordination of Al in zeolites. However, quantification of Al in different environments is difficult due to the second-order quadrupolar effects which arise because Al is a spin 5/2 nucleus.[11−14] These effects can be reduced by hydrating the sample, which relaxes the strain around an Al atom, thereby placing the Al nucleus in a more symmetric environment, and by using MQMAS techniques in combination with high magnetic field strengths.[11,15,16] These methods have been used to identify the distribution of tetrahedrally and octahedrally coordinated Al.[11−14,16−19] ^{27}Al MAS NMR has been used recently to characterize dehydrated zeolites;[20] however, to the best of our knowledge there have been no reports of in-situ ^{27}Al MAS NMR spectra dehydrated zeolites acquired at high temperature. The presence of paramagnetic species, such as Cu^{2+} and O_2, results in line broadening of ^{27}Al NMR lines, further complicating the interpretation of this technique.[21,22] Recently, work by two groups has shown that Al K-edge X-ray absorption near edge spectroscopy (XANES) analysis can be used to determine the distribution of Al between tetrahedral and

* To whom correspondence should be addressed. Tel: 510-642-1536. Fax: 510-642-4778. E-mail: bell@cchem.berkeley.edu.
[†] Department of Chemical Engineering, University of California, Berkeley.
[‡] Chemical Sciences Division, Lawrence Berkeley National Laboratory.
[§] Department of Chemistry, University of California, Berkeley.
[||] University of Nevada.
[⊥] Lawrence Berkeley National Laboratory
[#] Fukuoka University.

10.1021/jp058244z CCC: $33.50
Published on Web 05/28/2006

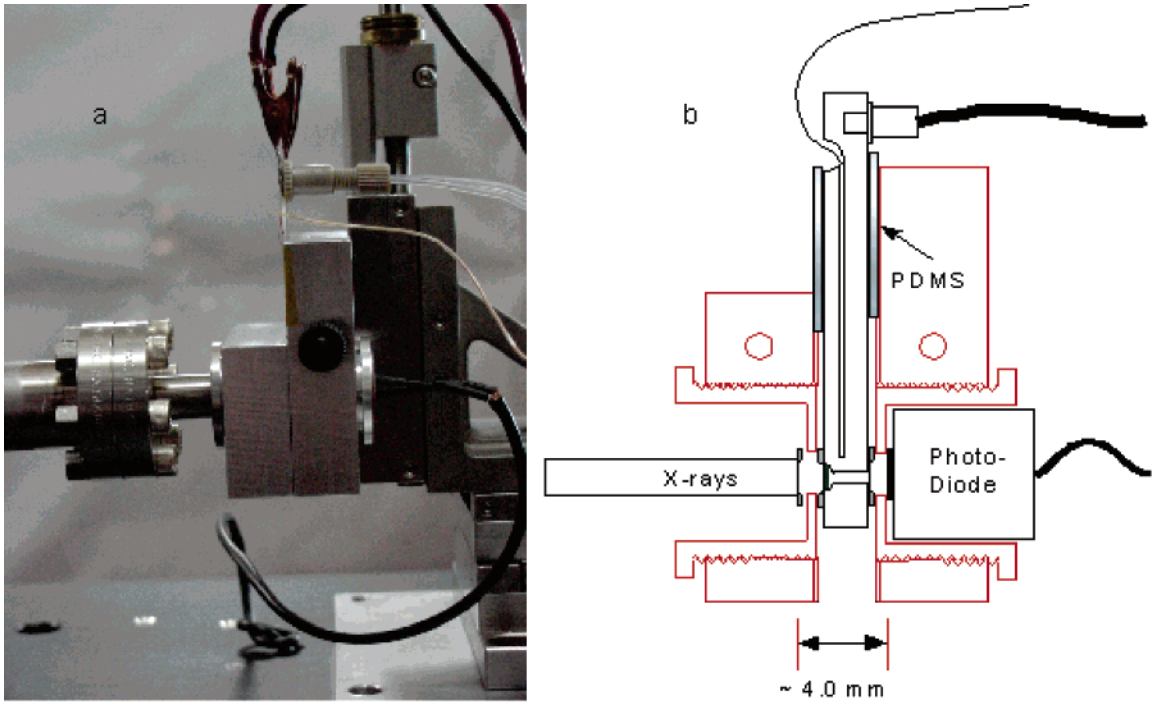

Figure 1. (a) Picture of in situ cell in position for transmission experiment at BL 6.3.1. (b) CAD drawing of in-situ cell and holder. The horizontal scale of the in-situ cell is expanded to show detail; however, the aluminum holder, beamline, and detector are drawn to scale.

octahedral coordination sites in both hydrated and dehydrated zeolite samples.[23−27]

Our group has recently developed an in-situ cell for acquiring XAS data using soft X-rays (200 and 2000 eV).[28] This cell has a path length of 0.8 mm and can operate at 1 atm at temperatures up to 773 K. We have used this cell in the present work to explore the local environment of Al in USY and ZSM-5. Both zeolites were examined in their ammonium-, proton-, and copper-exchanged forms. It was of particular interest to establish the effects of temperature on the local coordination of Al and the Al−O bond distance when different cations are used for charge compensation. An additional objective was to demonstrate that Al K-edge EXAFS data can be used to determine the Cu−Al distance in Cu−USY and Cu−ZSM-5. Infrared spectroscopy and ^{27}Al MAS NMR were used as complementary techniques to support the findings obtained by Al K-edge XAS.

Experimental Section

General. NH_4-ZSM-5 (Si/Al = 12) and NH_4−USY (Si/Al_{total} = 2.6) were obtained from ALSI-PENTA Zeolithe GmbH and Englehard, respectively. NH_4−Y (Si/Al = 2.6) was obtained from Strem Chemicals. Standards for Al XAS included a 0.4 μm Al foil, amorphous Al_2O_3 (Aldrich), and γ-alumina (Aldrich). The Al content was determined by Galbraith Laboratories (Knoxville, TN) using inductively coupled plasma (ICP) analysis. Initial assessment of zeolite and standard quality, prior to analysis by XAS, was determined using characterization by PXRD and N_2 porosimetry.

Materials Preparation. 1.0 g of NH_4−USY (ZSM-5) was oven dried at 393 K for 5 h. The oven dried material was then converted to H−USY (ZSM-5) by heating a shallow bed of the zeolite in a quartz reactor (zeolite height = 5 mm, reactor diameter = 20 mm). The temperature was ramped to 823 K at 1 K min^{-1} in a He flow of 50 cm^3 min^{-1}. The temperature was held isothermal at 823 K for 6 h. The as-prepared H−USY was then stored in a N_2 drybox. Cu^+-exchanged zeolites were prepared by mixing 500 mg of dry H−USY (ZSM-5) with enough CuCl (mp = 703 K) to achieve a value of Cu/Al = 1. The CuCl was ground in the drybox with a mortar and pestle to obtain a fine powder, which was then mixed with H−USY and ground again. The zeolite and CuCl mixture was placed in the quartz reactor in the N_2 drybox, sealed, and transferred to the exchange apparatus. The physical mixture was heated to 923 K at 1 K min^{-1} in a He flow of 50 cm^3 min^{-1}. The exchange temperature was held constant at 923 K for 15 h. The final yellow/tan colored material was stored in a N_2-purged drybox until further use.

Al K-Edge X-ray Absorption Spectroscopy (XAS). Al K-edge EXAFS and XANES data were acquired on beamline 6.3.1 at the Advance Light Source (ALS) at the Lawerence Berkeley National Laboratory (LBNL).[29] This is a bending magnet beamline with focusing optics and a Hettrick−Underwood-type, varied-line-space (VLS) grating monochromator with a useable energy range between 200 and 2100 eV.[29] The grating monochromator (2400 l/mm) has an energy resolution of $\Delta E/E$ = 5000. The pre-monochromator vertical aperture of the beam was set to 40 μm to optimize flux and resolution. The beam size at the sample was approximately 100 × 40 μm. Transmitted light of higher energies resulting from allowed orders of diffraction from the monochromator were not detected because the flux drops precipitously above 2100 eV. The ALS ring operated at 1.9 GeV. During experiments, data were taken with ring currents between 200 and 400 mA. Al metal foil (0.4 μm) was used for initial energy calibration (1559 eV). A newly designed end station allows for experiments at atmospheric pressures.[30,31]

An in situ cell,[28] designed for transmission and fluorescence experiments, was used with a newly designed holder shown in Figure 1. The cell is held in position by two aluminum blocks attached to a Newport *xyz* stage (see Figure 1a). Each aluminum block has a 20 mm threaded hole. Caps were designed with a groove for holding a 10.0 mm framed Si_3N_4 window and a poly(dimethylsiloxane) (PDMS) washer at its outer diameter. These caps are screwed into the aluminum blocks and form a

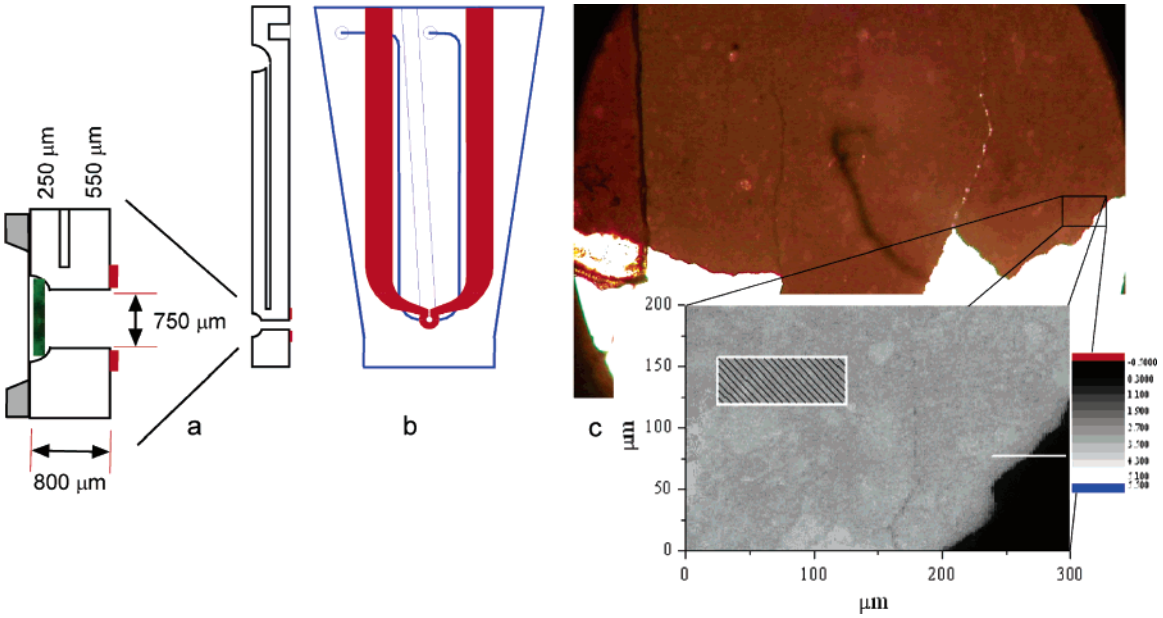

Figure 2. (a) Cad drawing of pellet placement in the in situ cell. Distances are given for reference. (b) Cad drawing of the in situ cell. (c) Light-microscope image of NH_4−USY pellet. Expanded region shows an X-ray optical density profile (1580 eV) of an area of the pellet (200 μm × 300 μm) investigated by STXM. Scale to right shows optical densities. Boxed region with diagonal lines represents the expected X-ray beam size at the sample (40 μm × 100 μm).

compression fitting for the Si_3N_4 windows onto the glass in situ cell. The low thermal conductance of SiO_2 combined with the high thermal conductance of Al allows the PDMS washer to remain intact, even when the central heated region exceeds 773 K. With the arrangement shown in Figure 1b, the total path length between the beamline termination and the detector is ∼4 mm, of which ∼0.8 mm is within the in situ cell. All of the components shown in Figure 1b are enclosed in a black acrylic box (30 × 15 × 15 cm) to prevent stray light from illuminating the photodiode detector (discussed below). To minimize atmospheric absorption in dead volume between beamline exit and detector, the acrylic box is continually flushed with He. A portable flow manifold was used to treat the catalysts on-site.[28] Samples of H^+ or Cu^+-exchanged ZSM-5 and USY were first treated in He (99.999%) at a flow rate of 5 cm^3 min^{-1}. The temperature was increased in increments of 15 K to 573 K (or to a limiting temperature established by the design of the heating element) and maintained isothermal at each temperature for the time it takes for one scan (5 min). Following heating, the sample and cell were cooled to room temperature and He saturated with water vapor was introduced. The temperature range was determined by the power supply and resistance of heater used. A new cell was used for each experiment.

Samples for transmission XAS experiments were prepared by pressing self-supporting pellets. Sufficient quantity of each sample was weighed to give an absorbance ($\mu_m \rho x$, where μ_m is the mass absorption coefficient [g cm^{-2}], ρ is the sample density [cm^3 g^{-1}], x is the X-ray path length) between 1.5 and 3.0 calculated[32] at +20 eV above the absorption edge.[33] Typically 7−10 mg of zeolite sample was pressed into a 20 mm diameter (2.2−3.2 mg cm^{-2}) pellet at 15 000 psi.

A 2 mm diameter fragment of a pellet was loaded into the in situ cell under ambient conditions. The open ends of the sample compartment (Figure 2a, 2b) were closed by Si_3N_4 windows (Silson Ltd.). The windows are 100 nm thick and cover an area of 1.5 mm × 1.5 mm on a 10.0 mm frame. Compression end caps (see above) were used to attach the windows to the cell body. The cell was then connected to the gas manifold and the sample was flushed with dry He (99.999%). A detector (4.6 × 4.6 mm photodiode, Hamamatsu, G1127-02) was installed in one of the compression end caps to measure the attenuated transmitted photon flux.

With the exception of Al foil, Al standards were too thick optically to use pellets for transmission experiments. These materials were therefore measured by either total electron yield or fluorescence in a vacuum chamber (10^{-8} Torr) located downstream of the atmospheric endstation. The signals obtained in this fashion were 2−3 orders smaller in intensity compared to those obtained in transmission. Standards for total electron yield were prepared by deposition onto carbon tape. A thin Al foil estimated at 0.4 μm thick (based on absorption) was also used in the vacuum chamber.

Beam intensities were measured over a 330 eV range (1510 to 1840 eV). An energy step of 0.5 eV was used, and five points were averaged at each energy step. A single scan could be completed in 5 min with very high signal-to-noise ratio (∼300). All in situ data were checked for reproducibility. For vacuum work, 2−3 scans were taken of a particular sample. Each file contained an I_0 reading measured as the drain current from a silicon vertical refocusing mirror (M3) placed after the monochromator under vacuum.[29] The mirror contained traces of Si. The Si edge at 1839 eV was used for internal calibration of the data.

The uniformity of the optical density of the sample pellet was determined with a scanning transmission X-ray microscope (STXM) which mapped the optical density (OD) for specified regions.[34] Figure 2c shows an image of the NH_4−USY (300 μm × 200 μm, with 0.5 μm/pixel resolution) obtained just above the Al K-edge, at 1580 eV. Pixels in this image measure the X-ray photon intensity, I_p, where p is the pixel number. The incident flux, I_0, was determined by taking the average photon count where no sample was present (black region of Figure 2c). Pixels were converted to absorbance or optical density by calculating the $\ln(I_p/I_0)$ at every pixel. Figure 3 shows the OD image of the same area. The variation in optical density over the entire image is plotted as a histogram in Figure 3a. The average OD density is 3.0 and the variance in optical density variation is small. If one considers a region representative of

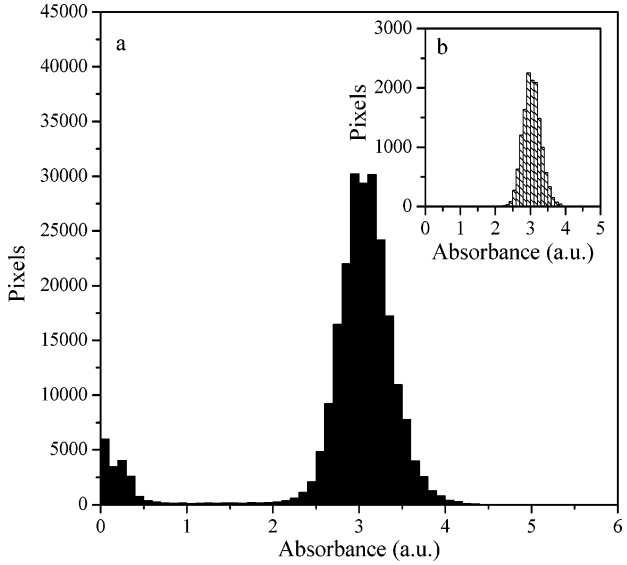

Figure 3. (a) Histogram of the absorbance variation in the pixels of the 200 μm × 300 μm STXM image shown in Figure 2c. (b) Histogram of the absorbance variation in the pixels of the 100 μm × 40 μm box represented in Figure 2c.

the beam size at BL 6.3.1 of the ALS (40 × 100 μm), a near constant OD is observed as shown in Figure 3b. Determining the uniformity of the sample optical density is critical for quantitative X-ray absorption experiments and eliminates concerns about pinhole effects.[35] All of the image analysis described above was performed using Origin Pro 7.0.

Cl and Cu K-Edge XAS. Cl K-edge XANES measurements were performed on beamline 9.3.1 of the Advanced Light Source (ALS) at the Lawrence Berkeley National Laboratory. This beamline is equipped with a Si (111) double crystal monochromator. Samples were loaded on 1 cm × 1 cm plates and loaded into the sample chamber of the endstation, which was operated at 10^{-7} Torr. No windows isolated the endstation from the beamline in normal operation. A silicon photodiode (Hamamatsu model 3584-02) detector could be maneuvered at a 45° angle relative to the incident radiation within 2−5 mm of the sample face in order to measure X-ray and visible fluorescence. An electrometer (Keithley 6517A) was used to amplify the measured photodiode current. All energies were referenced to the Cl K-edge of Cs_2CuCl_4.[36−38] The maximum of the first edge-region feature in the spectrum of this material is 2820.20 eV. Scans were made between 2700 and 2923 eV with a 0.1 eV step in the edge region. Other details concerning data acquisition and analysis can be found in ref 39.

Cu K-edge XAS measurements were performed at the Stanford Synchrotron Radiation Laboratory (SSRL) on beamline 2-3, which is equipped with a Si (111) double crystal monochromator. The pre-monochromator vertical aperture of the beams was set to 0.5 mm for improved resolution, defining an energy resolution of 1.8 eV. The monochromator was detuned 20−30% at 400 eV above the Cu K-edge to attenuate the flux from higher order Bragg diffractions. Cu metal foil (7 μm) was used for energy calibration and changes in beam alignment.

Each sample was pressed into a rectangular pellet (0.43 × 1.86 cm, with the thickness dependent upon the amount of sample used) and loaded into an in situ cell for hard X-ray transmission experiments.[40] Sufficient quantity of each sample was used (typically 5−10 mg for standards and 50−80 mg for samples) to give a calculated optical density ($\mu_m \rho x$) of 2.[33] Intensities of the beam were measured over a 900 eV range using a sampling step of 5 eV in the pre-edge and 0.3 eV in the XANES region (−30 to 30 eV relative to E_0), with a 1 s hold at each step. Other details concerning data acquisition and analysis can be found in ref 41.

Al K-Edge XANES Analyses. Al XANES data analysis was performed using Origin Pro 7.0. The energy was calibrated using the Si K-edge of the Si contaminant on the M3 mirror,[29] which appears at 1839 eV. Bulk absorption of Si, O, and Al as well as the atmosphere between the exit window of the beamline and detector in the pre-edge region were subtracted using a linear fit to the data in the range of −50 eV to −20 eV, relative to the sample edge energy (E_0). Each spectrum was normalized to an edge step of 1 using the absorption at +50 eV relative to E_0. The edge-energy of each sample and reference was taken at the first inflection point on the rising absorption edge.

Al K-Edge EXAFS Analyses. Al K-edge EXAFS data analysis was performed using the UWXAFS[42] suite of software programs and its GUI-based equivalent, IFEFFIT.[43] The AUTOBK background fitting algorithm was used.[44] A background function was subtracted from the normalized data using spline points between a wavenumber (k) of 0.5 Å^{-1} and 8.36 Å^{-1}. A strong spline clamp was made to the point at 8.36 Å^{-1}. An R_{bkg} value of 1.0 was chosen. Non-phase-corrected Fourier transforms (FTs) were performed on the k^1- and k^3-weighted $\chi(k)$ functions. Weighting of data with k^3 magnifies the presence of Cu, which has its largest backscattering amplitude at high k.[33b,d] Figures showing FT $k^3\chi(k)$ or FT $k^1\chi(k)$ data are plotted without phase correction. All spectra, except those of H−ZSM-5, were fit in R-space between 0.5 Å and 1.95 Å following FT between 2.25 and 7.5 Å^{-1} with a Hanning window function and a window sill width (dk) of 1 Å^{-1}. The data for H−ZSM-5 were fit in R-space between 0.8 Å and 1.95 Å following FT between 2.25 and 7.5 Å^{-1}. The above transform ranges define the number of relevant independent variables ($N_{ind} = 2\Delta R\Delta k/\pi + 2$) as approximately 6.

S_0^2 was extracted by fitting the first peak in FT $k^3\chi(k)$ for Al foil, using the theoretical values of $F_j(k)$ and $\phi_j(k)$ determined by the FEFF8.2 code.[45,46] The fit assumes that the Debye−Waller factor (σ^2) can be modeled using the correlated Debye model.[47] The correlated Debye model requires the Debye-temperature (θ_D) as an input. θ_D has been previously reported for Al metal (θ_D = 410 K at 298 K).[48] The fit of S_0^2 was done in R-space and k-space. A value of $S_0^2 = 0.86$ was obtained in both refinements and this value was used in all subsequent analyses.

All fits of samples and standards were performed on the real and imaginary parts of the FT $k^1\chi(k)$ data. A goal of the present study was to get quantitative information on the change in coordination number (CN) as samples dehydrate. The error in CN determination is often cited as ±25%.[49] However, ^{27}Al MAS NMR allows for a calibration point of the EXAFS amplitude dependent terms of CN and σ^2. Since Al in NH_4-ZSM-5 was found to be exclusively 4-coordinate by ^{27}Al MAS NMR, the value of CN was set at 4 in order to determine σ^2 more reliably. A value of 0.001 Å^2 was found for σ^2 and set constant in the fitting of all samples. In situ EXAFS data were fit with one Al−O shell by allowing the Al−O coordination number (CN_{Al-O}), radial separation of Al and O (R_{Al-O}) and the edge shift correction (ΔE_0) to vary as free variables ($N_{free} = 3$). The quality of a particular fit was evaluated by use of the reduced chi-square method (χ_ν^2),[50] and once a best fit was found, the $\mathcal{R}$-factor[50] was recorded for presentation of the fits. This factor gives a sum-of-square measure of the fractional misfit.[50,41] An upper bound in the error of CN_{Al-O} determination was made by making a second fit to the data setting σ^2, assuming that

this parameter varies linearly over the temperature range of interest with a slope of 3.6×10^{-6} Å^2 K^{-1}. This results in a doubling of σ^2 between 298 and 573 K. A doubling in σ^2 is predicted over this temperature range for Al metal.[48] However, since aluminum oxides (such as Al_2O_3, mp = 2326 K, θ_D = 1045 K[51]) have melting points much higher than Al metal (mp = 933 °C), the temperature dependency of σ^2 for zeolites is not expected to be as great as that for Al metal, since oxide supports have lower Debye−Waller factors than metals.[52]

FEFF Simulations. To model the effects of Al−Cu separation and Cu/Al ratio on the EXAFS scattering function, a FEFF8.2 simulation was performed on a Cu^+ cation located near an Al atom situated in the T12 site of ZSM-5. The initial positions of all atoms in the 34-atom cluster representing the Cu^+ cation and the T12 cation exchange site were taken from a DFT study of Cu-exchanged ZSM-5.[53] This cluster is referred to hereafter as the T12 cluster. Scattering paths were calculated using calculated atomic potentials contained in the FEFF8.2 code.[46] Paths were calculated initially setting S_0^2 to 0.0 and σ^2 to 0.0 Å^2. 50 to 150 paths were generated for total path lengths of less than 6 Å. For initial comparison to experimental spectra, all paths of a particular model were summed assuming S_0^2 = 0.86, σ^2 = 0.001 Å^2, ΔE = −9.0 eV and ΔR = 0.0 Å. These values were determined from fits to experimental spectra. Subsequent analysis revealed that multiscattering paths greater than three segments have a negligible contribution and that the main features of the spectrum can be described almost exclusively by scattering paths with three or fewer path segments with a total path length less than 3.5 Å.

The Al−O path for the CuT12 cluster (1.68 Å) was used to fit the Al−O shell for all data. EXAFS structural parameters were taken initially from best fit results for NH_4-ZSM-5. The following values were used for all of the FEFF simulations: ΔE_0 of −5.0 eV for all paths, σ^2 = 0.001 Å^2 for the Al−O path, σ^2 = 0.01 Å^2 for the Al−Si path, R_{Al-Si} = 3.04 Å, and CN_{Al-Si} = 4. These values were determined from a separate fit of the first shell (Al−O) and second shell (Al−Si) of NH_4-ZSM-5. To model the effects of Al−Cu separation and Cu/Al ratio on the spectrum, σ^2 is assumed to be 0.001 Å^2 for the Al−Cu path. The value of CN_{Al-Cu} was set initially at 1.0 and the value of R_{Al-Cu} was varied between 2.71 Å and 2.87 Å. In a second simulation, the value of R_{Al-Cu} was set at 2.79 Å and the value of CN_{Cu-Al} was varied between 0 and 1.

FTIR. Samples (1−2 g) of NH_4-exchanged ZSM-5 and USY were converted to H-exchanged ZSM-5 and USY by heating the samples from 298 to 823 K at 1 K min^{-1} in a shallow bed reactor (reactor diameter/catalysts height = 2/1) using 50 cm^3 min^{-1} He. Self-supporting pellets (∼ 5−8 mg cm^{-2}) of Cu- and H-exchanged ZSM-5 and USY were prepared in ambient atmosphere using a hydraulic press. All pellets were then activated by removing the ambient water by heating the pellets from 298 to 723 K at 1 K min^{-1} in He using a high-temperature infrared cell similar to that described by Joly et al.[54] A Thermo-Nicolet NEXUS 670 spectrometer was used to acquire all infrared spectra. Typically, 32 scans were averaged using 2 cm^{-1} resolution. Two BaF_2 windows were used to seal the cell. The cell windows provided a usable energy range extending to 1200 cm^{-1}.

To determine the framework content of Al in USY, infrared spectra were taken of the zeolite. Both NH_4−USY and NH_4−Y were studied for comparison. Thin self-contained pellets of 2−3 mg cm^{-2} were prepared as above; however, a cell was not used for these measurements. This allowed resolution of the framework stretches below 1000 cm^{-1} and extended the usable energy range to 550 cm^{-1} limited only by the IR source itself.

^{27}Al MAS NMR. Samples of NH_4-, H-, and Cu-exchanged ZSM-5 and USY were stored in a container with 1 M NH_4NO_3(aq) and equilibrated with H_2O(v) (1.97 kPa at 298 K) overnight. 40−70 mg of sample were loaded into a 4 mm diameter zirconia rotor and sealed with a Kel-F cap. The ^{27}Al MAS NMR spectra were collected using a Bruker 500 (11.7 T) spectrometer equipped with a 4 mm MAS probe. The ^{27}Al signals were referenced to external aqueous $Al(NO_3)_3$ and used to calibrate the 90° flip for nonselective irradiation of all aluminum transitions. The ^{27}Al MAS NMR spectra of all zeolite samples were acquired using a 15° flip angle; 2000 scans were accumulated using a 1 s pulse delay. The MAS spinning speed was 12.0 kHz.

Results and Discussion

Physical Characterization of NH_4-, H-, and Cu-Exchanged USY and ZSM-5. XRD of NH_4-, H-, Cu−USY and ZSM-5 show the expected patterns of USY and ZSM-5 zeolite respectively with no indication of Al_2O_3. Based on elemental analysis of USY the Si/Al ratio is Si/Al = 3.7, and exchange with CuCl, the Cu/Al and Cl/Cu ratios are Cu/Al = 0.64 and Cl/Cu = 0.13. CuCl was not detected by XRD; however, occluded CuCl was detected by Cl K-edge XANES, as discussed below. Elemental analysis of ZSM-5 gives a Si/Al ratio of Si/Al = 13.0, and, after exchange with CuCl, the Cu/Al and Cl/Cu ratios are Cu/Al = 1.65 and Cl/Cu = 0.2. In this case, both XRD and XANES showed evidence for occluded CuCl. Assuming that the occluded CuCl corresponds to Cu/Al = 0.33, then the ratio of exchanged Cu per Al is 1.32. The excess of Cu (i.e, Cu/Al = 0.32) is believed to be present as either CuOH or Cu_2O.

The framework ratio of Si to Al in USY was estimated on the basis of the frequency of the TO stretching. This feature was observed at 820 cm^{-1} for NH_4−USY and at 792 cm^{-1} for NH_4−Y. Using published values for the position of this band as a function of Si/Al in the framework,[55] the ratio of framework Si to Al was estimated to be 6 ± 1. Therefore, if the degree of Cu^+ exchange is recalculated on the basis of framework Al, the Cu-to-Al ratio is 1.01. For Cu−ZSM-5, all of the Al atoms are taken to be in the zeolite framework.

Further evidence for the complete exchange of Cu^+ cations with hydroxyl groups in H−ZSM5 and H−USY comes from the results shown in Figure 4. The FTIR spectra of the OH stretching region for H−USY and -ZSM-5 indicate both Si−OH and bridging OH Brønsted sites in these materials. The bands observed at 3734, 3711, and 3587 cm^{-1} for H−ZSM-5 are assignable to silanol OH groups, OH groups interacting with extraframework Al species,[56] and Brønsted acid, bridging OH groups.[57] The peak at 3734 cm^{-1} observed in the spectrum of H−USY is also assigned to silanol OH groups, whereas the peaks appearing in the region of 3675−3450 cm^{-1} are attributed to various types of Brønsted acid hydroxyl groups.[58] Following exchange with CuCl, nearly all of the bands for hydroxyl groups associated with Brønsted acid protons are removed in the spectrum of both Cu−USY and Cu−ZSM-5. The intensity of the silanol peak in both materials is smaller than in their respective proton forms, suggesting the formation of some Cu−O−Si structures.

Each of the zeolite samples was characterized by ^{27}Al MAS NMR, following standard sample hydration. The spectra presented in Figure 5 show that each sample has a prominent peak centered between 58 and 60 ppm that can be assigned to

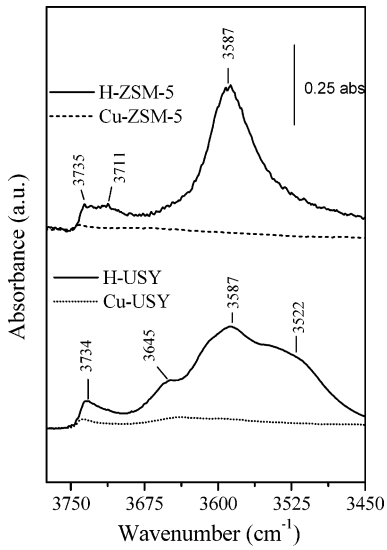

Figure 4. FTIR spectra of hydroxyl groups showing in-situ prepared H−USY and H−ZSM-5 and their Cu-exchanged forms. Spectra recorded at 723 K.

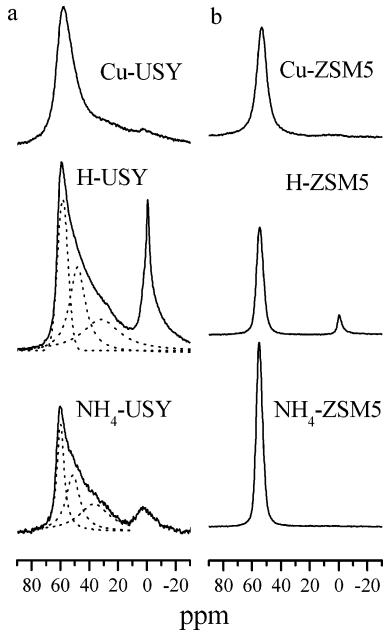

Figure 5. ^{27}Al MAS NMR of hydrated samples: (a) Cu−USY, H−USY, and NH_4−USY. The tetrahedral peak near −60 ppm of the H−USY and NH_4−USY spectrum is shown deconvoluted with three Gaussian functions. (b) Cu−ZSM-5, H−ZSM-5, and NH_4−ZSM-5.

tetrahedrally coordinated framework Al.[59] The peak at 58−60 ppm for NH_4−USY, H−USY, and Cu−USY has a broad tail. Deconvolution of the tail suggests that it is composed of two peaks centered at 30 and 50 ppm. Previous studies have proposed that similar peaks may be due to pentacoordinated Al in extraframework structures.[59] A peak at 0−3 ppm is also observed in all three USY samples. This peak has been assigned to octahedrally coordinated Al, which may either be present as extraframework Al[60] or in the zeolite framework.[61] If the peaks at 30 and 50 ppm are assigned to extraframework Al, then the fraction of all Al in USY within the zeolite framework is estimated at 60%, in very good agreement with the estimate obtained from the TO stretching vibrational peak measured by infrared spectroscopy. Upon conversion of NH_4−USY to H−USY, the peak for octahedrally coordinated Al increases considerably, but when protons are exchanged by Cu^+ cations followed by hydration, this peak is largely removed. In contrast to NH_4−USY, NH_4−ZSM-5 shows only a single symmetric peak for tetrahedral Al and no octahedral component. Conversion of NH_4-ZSM-5 to H−ZSM-5 leads to the appearance of a small peak at 0−3 ppm, but this feature disappears completely upon exchange of protons for Cu^+ cations followed by sample hydration.

XAS Characterization of H−ZSM-5 and H−USY. In situ XANES measurements of H−ZSM-5 and H−USY are shown in Figure 6. Hydrated H−USY exhibits two prominent peaks in the absorption spectrum shown in Figure 6a. The first peak at 1568.0 eV is characteristic of tetrahedrally coordinated Al in zeolites,[23,62−65] whereas the second peak at 1571.0 eV is characteristic of octahedrally coordinated Al.[23,62−65] The position of these peaks is listed in Table 1 together with standards reported in the literature. As the temperature is raised from 298 to 473 K, the peak at 1571 eV decreases in intensity and the peak at 1568 eV increases in intensity. An isosbestic point is observed at 1575.0 eV for H−USY. Similar trends were observed for H−ZSM-5 and are shown in Figure 6b. Rehydration of all samples following treatment at 573 K in He gave spectra similar to those of the initially hydrated materials. It is evident that H−USY still has some octahedrally coordinated Al at 473 K, even after it has been dehydrated. H−ZSM-5 shows similar intensities for tetrahedrally and octahedrally coordinated Al as those observed for NH_4-ZSM-5, suggesting all Al is tetrahedrally coordinated following dehydration. Differences in the intensity of the XANES signals are observed above 1575 eV for H−USY and H−ZSM-5 that have been attributed to differences in the long-range ordering of the two zeolites.[62]

Al K-edge EXAFS of H−USY and H−ZSM-5 were obtained in order to quantify the changes in the local structure of Al with dehydration. Figure 6c shows a series of $k^1\chi(k)$ spectra taken between room temperature and 473 K for H−USY, and Figure 6d shows a similar set of spectra taken between room temperature and 573 K for H−ZSM-5. The H−USY series exhibits four prominent isosbestic points at 1.6, 2.5, 3.3, and 4.5 $Å^{-1}$, suggesting that the Al coordination changes upon dehydration. The results for H−USY are qualitatively consistent with those reported recently in an in situ Al K-edge XANES study of the dehydration occurring in vacuo.[27]

Figure 7 shows the changes in the values of CN_{Al-O} backscattering and the R_{Al-O} as functions of the dehydration temperature for both H−USY and H−ZSM-5. Both parameters were obtained by fitting the EXAFS data obtained at different temperatures, assuming a single shell of O atoms surrounding each Al absorber. Also shown in Figure 7 is the amount of water remaining on the H−USY after dehydration at each temperature, expressed as the mole of H_2O per Al atom. For H−USY the value of CN_{Al-O} decreases monotonically from 5.0 toward 4.0 as the temperature increases from 298 K toward 473 K. This change is accompanied by a decrease in the amount of adsorbed water from $H_2O/Al = 2.2$ toward zero, and a decrease in R_{Al-O} from 1.71 A to 1.69 Å. The measured amount of adsorbed water also contains a contribution from physisorbed H_2O interacting with the oxygen framework. An attempt to correct for physisorbed water was made by repeating the experiment using Cu−Y, since the sample is virtually free of Brønsted protons (Figure 4). This experiment revealed 0.6 molecules of physisorbed H_2O are retained per Al atom. Therefore, it is estimated that 1.6 H_2O molecules per Al in H−USY are involved in strong interactions with Brønsted acid sites. If it is assumed that the majority of the Al is present in either tetrahedral or octahedral environments, then the values of CN_{Al-O} measured at 298 K suggest that 50%

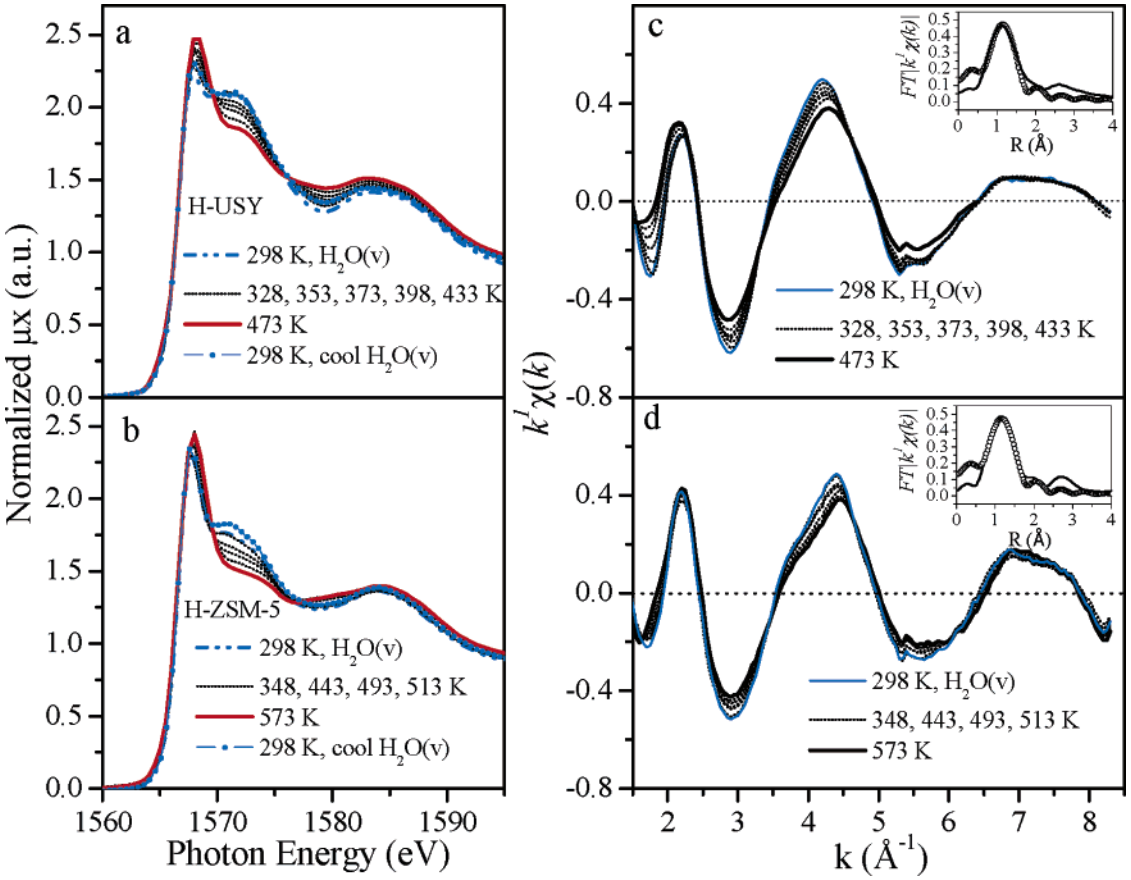

Figure 6. In situ Al K-edge XANES and EXAFS of proton form of zeolites USY and ZSM-5. All samples were initially equilibrated with water vapor before heating in dry He. Normalized Al K-edge XANES of (a) H−USY and (b) H−ZSM-5 shown over indicated temperature range. Spectra plotted on the same scale for intensity comparison. Al K-edge EXAFS of (c) H−USY and (d) H−ZSM-5 shown over indicated temperature range. Inset of (c) shows $FT|k^1\chi(k)|$ of H−USY at 433 K with the respective fit (open circles). Inset of (d) shows $FT|k^1\chi(k)|$ of the H−ZSM-5 at 443 K with the respective fit (open circles).

TABLE 1: Peak Positions Observed in Al K-Edge XANES of Standards and Zeolites

sample	peak positions (eV)	Al coordination[a]
NH_4^+ZSM-5	1567.0	4
NH_4^+USY	1567.0, 1570.0	4,6
γ-Al_2O_3	1567.0, 1568.5, 1571.5	4,6[b]
α−Al_2O_3	1568.5, 1572.5	6[b]
H−USY (298 K, hyd[c])	1567.0, 1571.0	4,6
H−USY (473 K, dehyd[c])	1567.0	
Cu−USY (298 K, hyd)	1567.0, 1571.0	4,6
Cu−USY (573 K, dehyd)	1567.0	
H−ZSM5 (298 K, hyd)	1567.0, 1571.0	4,6
H−ZSM5 (573 K, dehyd)	1567.0	
Cu−ZSM5 (298 K, hyd)	1567.0, 1571(Shoulder)	4
Cu−ZSM5 (573 K, dehyd)	1567.0	

[a] Assigned using ^{27}Al MAS NMR spectra. [b] Assigned in ref 64. [c] Hyd = Hydrated, Dehyd = Dehydrated.

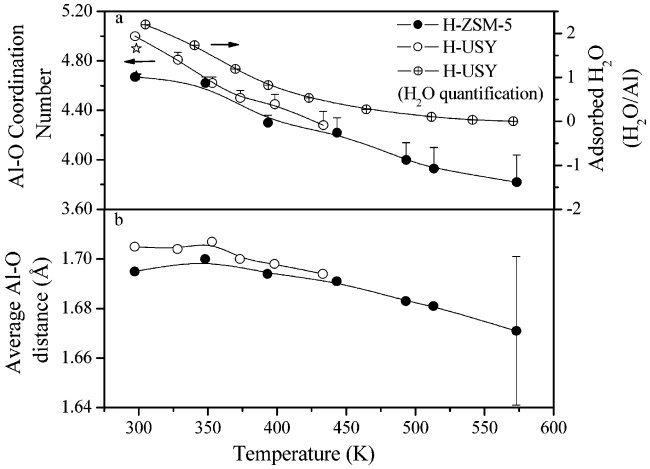

Figure 7. (a) Change in average Al−O coordination numbers with dehydration temperature for H−USY and H−ZSM-5. Positive error bars reflect the maximum upper bound on Al−O coordination assuming the Debye−Waller factor double between 298 and 573 K. Also shown is the water amount of water retained H−USY during a temperature-programmed desorption. Open and solid star represents CN_{Al-O} of rehydrated H−USY and H−ZSM-5, respectively. (b) The trend in average Al−O bond lengths with dehydration temperature for both H−USY and H−ZSM-5.

of the Al in H−USY is present in an octahedral environment, which is in reasonable agreement with the value determined from ^{27}Al MAS NMR, 44%. A complete set of structural results for the H−USY temperature series is shown in Table 2. Qualitatively similar trends for CN_{Al-O} and R_{Al-O} were observed for H−ZSM-5 shown in Table 3; however, in this case the dehydration temperature was raised to 573 K. In this case, the percentage of Al present in octahedral sites at 298 K is 33%, which is noticeably higher than that estimated from the ^{27}Al MAS NMR spectrum shown in Figure 5. While the values of CN_{Al-O} and R_{Al-O} for H−USY are higher than those for H−ZSM-5 at 298 K, they become virtually identical above 498 K, suggesting that the local environment of Al in the two zeolites is very similar once they are fully dehydrated. This might suggest that the intrinsic activity of each catalyst is the same. A recent study of *n*-hexane cracking catalyzed by zeolites of different crystal structures has led to the conclusion that the

TABLE 2: Fraction of Octahedral Al in H−USY Determined on the Basis of Average Coordination Numbers Obtained from Fitting EXAFS Data[a]

temp (K)[b]	CN[c]	X_{oct} [d]	R_{Al-O} (Å)[f]
298	5.0	0.50[e]	1.70
328	4.8 (0.06)	0.41 (0.02)	1.70
353	4.6 (0.05)	0.31 (0.03)	1.70
373	4.5 (0.06)	0.25 (0.04)	1.70
398	4.5 (0.08)	0.22 (0.06)	1.69
433	4.3 (0.11)	0.14 (0.08)	1.69

[a] All spectra fit in R-space using identical transform parameters. Free variable in fit, CN, Δr, ΔE_0. σ^2 found to be 0.001 Å^2 in fit for NH_4-ZSM-5. This value was fixed for all temperatures. Fitted value of ΔE_0 was −9(7) eV. [b] Data at 473 K were only taken to 6.5 k^{-1} and could not be fit reliably. [c] Fitted coordination number (CN). $CN = 6X_{oct} + 4X_{tet}$. Estimated errors in CN are positive in direction only and their values are shown in parentheses. [d] Estimated errors in X_{oct} are positive in direction only (directly correlated to error in CN) and their values are shown in parentheses. Errors determined by setting upper limit on σ^2 at each temperature using the Debye model. Procedure explained in text. [e] ^{27}Al MAS NMR results suggest 44% octahedral. [f] Fitting error on Al−O bond lengths are ± 0.04 Å.

TABLE 3: Fraction of Octahedral Al in H-ZSM-5 Determined on the Basis of Average Coordination Numbers Obtained from Fitting EXAFS Data[a]

gas treatment	temp (K)	$1s \rightarrow 4p_{x,y}$ [a] (eV)	$1s \rightarrow 4p$[b] (eV)	$1s \rightarrow 3d$[c] (eV)
He	673	8983.1	8994.5	–
MeOH/He	298, 363, 403	8982.8	8993.9	–
CO/He	298, 363, 403[d]	8981.1/8983.3	8994.6	–
	298	8981.1/8983.3	8993.4	8978.4
MeOH/CO/O_2	363	8981.1/8983.0	8992.8	8978.1
	403	8981.1/8982.7	8992.2	8977.8

[a] Peak energy in normalized first derivative spectrum. [b] Peak energy in normalized first derivative spectrum associated with highest energy adsorption in the white line. [c] Weak pre-edge peak associated with Cu^{2+} defined at the point of peak inflection. [d] Peak at 8982.0 eV forming

intrinsic acid strength of Brønsted acid centers in zeolites does not depend on the crystal structure of the zeolite.[66]

The values of CN_{Al-O} and R_{Al-O} determined in this study of NH_4−USY and NH_4−ZSM-5, and for dehydrated H−USY and H−ZSM-5 are compared in Table 4, with similar results reported in the recent literature for NH_4−Y[67] and dehydrated H−Y[24,67] and H−ZSM-5[24] in Table 5. Previous investigators have modeled the Al EXAFS spectrum with a much larger set of adjustable parameters than were used in the present work,[24] and hence have claimed that for dehydrated H−Y and H−ZSM-5 Al atoms in two shells could be defined: one for which $CN_{Al-O} = 3$, characterized by $R_{Al-O} = 1.66-1.68$ Å, and one for which $CN_{Al-O} = 1$, characterized by $R_{Al-O} = 1.87-1.98$ Å. Our experience has shown that a statistically meaningful fit cannot be achieved using more than six adjustable parameters and that, within this limitation, it was not possible to identify more than a single value of CN_{Al-O} and R_{Al-O}. Taking this point into consideration, it is evident that the values of CN_{Al-O} and R_{Al-O} obtained in the present work are comparable or slightly smaller than the average values reported previously for similar zeolites.

The progressive decrease in CN_{Al-O} and R_{Al-O} with increasing dehydration temperature and the reversibility of the effects of dehydration upon rehydration, suggest that the Al atoms attributed to octahedral sites by either ^{27}Al MAS NMR or Al K-edge XANES are, in fact, associated with the zeolite framework, rather than being extraframework. The decrease in the fraction of octahedrally coordinated Al upon dehydration reported here is consistent with that reported recently by Omegna et al. for H−Y and H−USY.[27] The authors of that study proposed that the observed effects H−USY are due to the interactions of H_2O with both framework Al and amorphous silica−alumina in the zeolites.[17,27] An illustration of the interaction of H_2O with framework, similar to that presented in ref 17, is shown in Scheme 1. We suggest that octahedrally coordinated Al atoms are framework Al atoms that interact strongly with three hydroxyl groups and a molecule of H_2O. This final state is formed through a process in which two water molecules adsorb and form a hydrogen bonding network with the Brønsted proton and an oxygen framework. This is illustrated in the center cartoon of Scheme 1. Quantum chemical studies have shown that such a structure would readily be formed upon the interaction of two molecules of H_2O with a single tetrahedrally coordinated framework Al atom.[68−70] Consistent with this interpretation we observe that the dehydration of H−USY occurs with the elimination of 1.6 molecules of H_2O per Al atom. This is reasonably close to what would be expected for the dehydration of octahedrally coordinated Al sites, if ∼50% of all Al sites are in this state of coordination for fully hydrated H−USY (1.0 molecule of H_2O per Al atom). The much lower level of octahedrally coordinated Al for NH_4−USY and NH_4−ZMS-5 observed at 298 K by both ^{27}Al MAS NMR and Al K-edge EXAFS (Table 4) is a result of the much lower degree of interaction of NH_4^+ cation with H_2O than of protons.

Table 6 lists the values of R_{Al-O} that have been determined for tetrahedrally coordinated Al by means of DFT calculations using a small cluster to represent the zeolite.[7,71,72] Two observations can be made. The first is that for NH_4−ZSM-5[72] and $(CH_3)_3PH$−ZSM-5[71] all four Al−O bond distances are nearly comparable, and the second is that for H−ZSM-5[71,72] and H−Y[7] one of the Al−O bonds is significantly longer that the other three. It is also observed that the average value of R_{Al-O} is 1.72 Å, which is about 0.05 A longer than the average values of R_{Al-O} found in this study. Given the uncertainties associated with the evaluation of R_{Al-O} from both Al K-edge EXAFS data and from DFT calculations, the level of agreement should be regarded as good.

XAS Characterization of Cu−ZSM-5 and Cu−USY. Figure 8 shows Al K-edge XANES spectra for Cu−USY and Cu−ZSM-5. Peaks at 1568 and 1581 eV for tetrahedrally and octahedrally coordinated Al, similar to those observed for H−USY and H−ZSM-5, are observed; however, the relative intensity of the peak for octahedrally coordinated Al is much less than in the case of the Cu-exchanged zeolites. These results are consistent with the ^{27}Al MAS NMR spectra shown in Figure 5 and are a direct consequence of the significantly weaker level of interaction of H_2O with Cu cations than with protons.[53]

Al K-edge EXAFS data ($k^3\chi(k)$) for Cu−USY and Cu−ZSM-5 are shown in Figure 9 and are compared with similar data for dehydrated H−USY and H−ZSM-5. It is immediately evident that the principal difference in the data for the H- and Cu- forms of the zeolites can be seen in the region of 6−8 Å^{-1}. When Cu^+ cations (see below) are exchanged for protons, backscattering from Cu becomes most important in the region noted. FEFF8.2 simulations of the Al K-edge EXAFS data for Cu−USY and Cu−ZSM-5 give values of $CN_{Al-O} = 4.1-4.2$ and $R_{Al-O} = 1.69-1.71$ Å, again showing no strong dependency in zeolite framework structure or temperature of zeolite dehydration. A value of CN_{Al-O} close to 4 even at 298 K is consistent with the Al K-edge XANES data presented in Figure 8 and is again indicative that the exchange of Cu^+ cation into both USY and ZSM-5 strongly suppresses the interaction of Al with H_2O.[53]

TABLE 4: Parameters Determined from Simulations of EXAFS Data for Cu−Y

method	treatment	shell	N^a	R (Å)^b	σ^2 ($\times 10^3$ Å)^c	ΔE_o (eV)^d	R-factor^e
Cu K-edge	He, 673 K	Cu−O	1.9 (2)	1.99 (1)			
	(Fit 1)	Cu−Si(Al)	1.2 (3)	3.12 (2)	5 (1)	1.2 (1.6)	0.018
	He, 673 K	Cu−O	2.2 (6)	1.98 (2)	7 (3)		
	(Fit 2)	Cu−Cl	0.1^f	2.14 (3)	0 (2)	−0.6 (2.2)	0.009
		Cu−Si(Al)	2.0 (1)	3.13 (2)	10 (5)		
Al K-edge	He, 523 K	Al−O	4.2 (6)	1.66 (4)		−13.6 (5)	0.072
		Al−Cu^h	1	2.87	1^g		

^{a} Coordination number. ^{b} Fitted radial distance. ^{c} Debye-Waller factor. ^{d} Energy reference shift. ^{e} R-factor. ^{f} Fixed value based on value determined for Cl/Cu determined by H_2-TPR. ^{g} Fixed value of $\sigma^2 = 10^{-3}$.[23] ^{h} Al−Cu distance was estimated based on FEFF 8.2 model discussed in text.

TABLE 5: Experimentally Determined Structural Values for Zeolites Y and ZSM-5

zeolite	CN (Al−O)	R_{Al-O} (Å)	σ^2 (Å^2)	ΔE_0 (eV)	ref
NH_4^+- Y	4.4 (7)	1.68 (3)	0.00 (set)	−2.7	67^a
H−Y (725 K, He)	3.1 (5)/1.1 (2)	1.66 (3)/1.89 (3)	−0.005 (5)	−3.1	67^a
H−Y (640 K, in vacuo)	3/1 (set)	1.68 (1)/1.87 (1)	0.006 (set)		25^b
H−ZSM-5 (640 K, in vacuo)	3/1 (set)	1.66 (1)/1.98 (1)	0.006 (set)		25^b

^{a} Fit with FEFF8 generated standard, path unknown. ^{b} EXCURVE simulation used for paths. Shortest and longest Al−O distance reported.

SCHEME 1

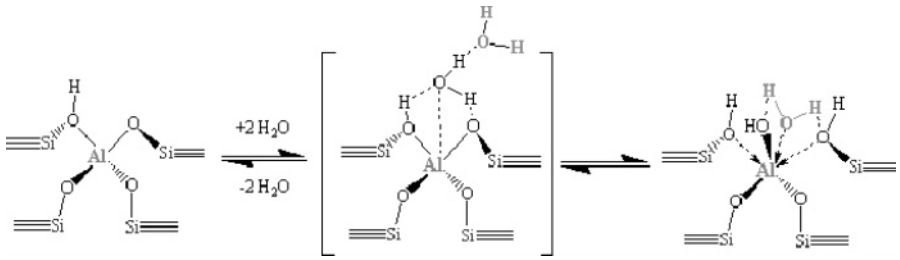

TABLE 6: Theoretically Determined Structural Values for Acidic and Copper Exchanged Form of ZSM-5 and Y Zeolites

	H−ZSM-5	H−ZSM-5	H−Y	NH_4−ZSM-5	$(CH_3)_3PH$−ZSM-5	Cu− ZSM-5	Cu− ZSM-5	CuT12	Cu−Y
$R_{Al-O(1ong)}$	1.827	1.983	1.900	1.839	1.725	1.753	1.79	1.756	
$R_{Al-O(short)}$	1.689	1.628^a	1.708	1.726^a	1.692	1.745		1.676	
R_{Al-O} (avg)	1.719	1.717	1.756	1.754	1.713			1.717	
R_{Cu-Al}						2.764	2.8	2.791	2.94
ref	71	72	7	72	71	74	75	53	76

^{a} Back-calculated using R_{Al-O} (avg) and $R_{Al-O(long)}$ assuming one short and three long bonds.

The oxidation state of Cu in Cu-exchanged USY and ZSM-5 was probed by Cu K-edge XANES. Figure 10 shows both absorption and first derivative spectra for Cu−USY and Cu−ZSM-5 in the as-prepared state, after exposure to ambient air and after dehydration in He at 598 K. All of the Cu in the as-prepared zeolites is present as Cu^+, indicating that cation exchange occurs via the process $Z^-H^+ + CuCl \rightarrow Z^-Cu^+ + HCl$. The complete disappearance of all Brønsted acid protons upon dry exchange with CuCl evidenced by infrared spectroscopy (see Figure 4) further supports this interpretation. When either Cu−USY or Cu−ZSM-5 is exposed to water vapor at 298 K, a part of the Cu^+ cations are oxidized to Cu^{2+}, as evidenced by a decreased intensity at 8983 eV and increased intensity of a peak at 8993 eV in the first derivative Cu K-edge XANES spectra of both zeolites. First derivative spectra of CuO and Cu_2O are also shown to highlight spectroscopic differences between Cu^+ and Cu^{2+}. Hydration, however, does not appear to lead to the demetalation of the zeolite, viz. $Z^-Cu^+ + 1/2\ H_2O \rightarrow Z^-H^+ + {}^1/_2\ Cu_2O(s)$.[53] Thermodynamic calculations have shown this pathway to be the most favorable due to the Madelung stabilization energy associated with the formation of the bulk oxide phase.[53] The occurrence of such a process would have led to the creation of a significant number of octahedrally coordinated Al sites via the interactions of additional water vapor with the newly formed Brønsted acid sites. The absence of evidence for such a change in the Al K-edge spectrum of both zeolites (see Figure 8) supports the conclusion that demetalation does not occur, even though theoretical calculations have suggested that this process is thermodynamically favorable.[53] Figure 10 also shows that dehydration of hydrated Cu−USY and Cu−ZSM-5 is partially, but not totally, reversible at 598 K.

An important question is whether the Cl retained in Cu−USY and Cu−ZSM-5 is associated with Cu or with Si or Al. It is recalled that elemental analysis indicates that the amount of Cl retained is equivalent to Cl/Cu = 0.13 for Cu−USY and Cl/Cu = 0.20 for Cu−ZSM-5. Cl K-edge XANES spectra were obtained to help identify the element to which Cl is bonded. Figure 11 shows Cl K-edge XANES spectra for the as-prepared Cu-exchanged zeolites. In both cases the form of the spectra is very close to that of CuCl, suggesting that, following exchange, Cl is retained as highly dispersed CuCl occluded in the pores of the zeolite. Upon hydration of the as-prepared Cu−USY, the Cl Kedge spectrum changes and becomes similar in shape to that of paratacamite, $Cu_2(OH)_3Cl$. The formation of $Cu_2(OH)_3$-Cl supports the idea that CuCl is occluded during Cu exchange with CuCl vapor, since $Cu_2(OH)_3Cl$ can be formed by reaction of CuCl with H_2O.[73] It should also be noted that the formation of $Cu_2(OH)_3Cl$ involves the oxidation of Cu^+ to Cu^{2+}, and hence

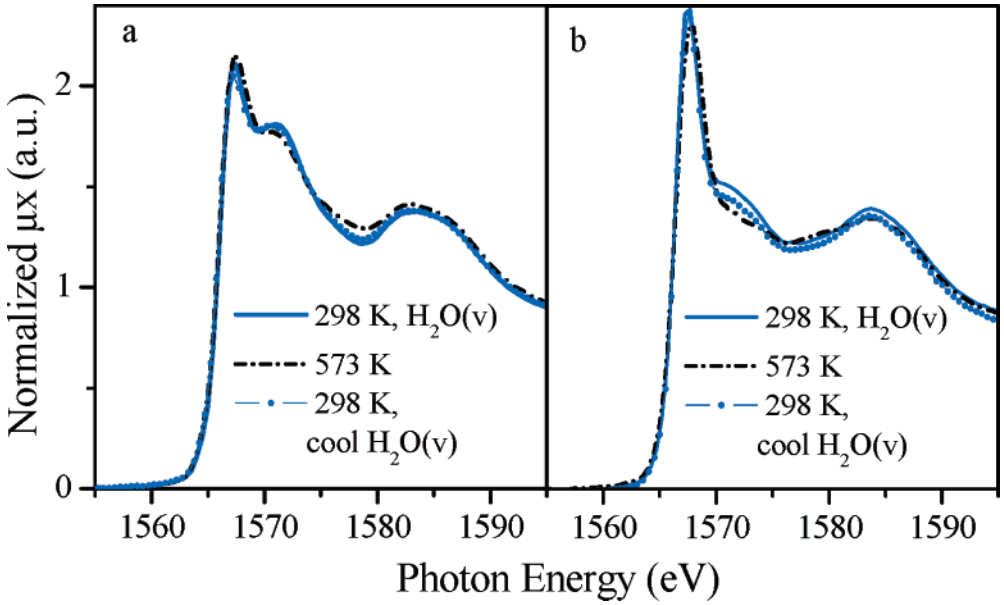

Figure 8. Al K-edge XANES study of Cu-exchanged zeolites: (a) Cu−USY, (b) Cu−ZSM-5. Cu-exchanged zeolites were hydrated at 298 K, heated in He to 573 K, and then cooled in wet He to 298 K.

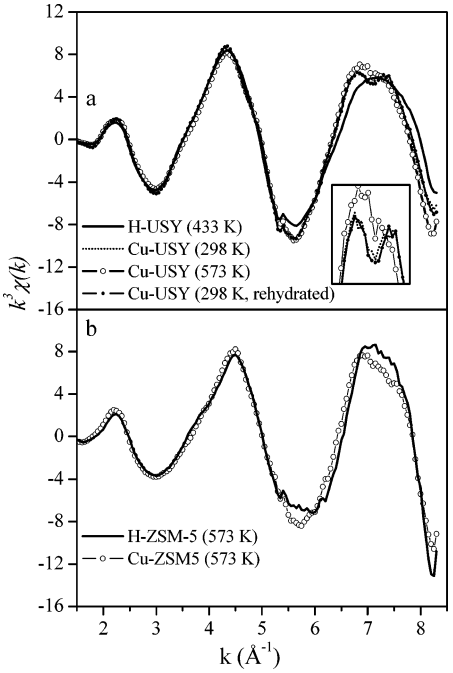

Figure 9. $k^3\chi(k)$ functions for He-treated H- and Cu-exchanged zeolites. (a) Comparison of H−USY (433 K), Cu−USY at 298 K, 573 K and cooled in $H_2O(v)$. Inset shows expanded region of in-situ treated Cu−USY between 6.5 and 7.5 Å^{-1}. (c) Comparison of $k^3\chi(k)$ of H−ZSM-5 (573 K) and dehydrated Cu−ZSM-5 (573 K).

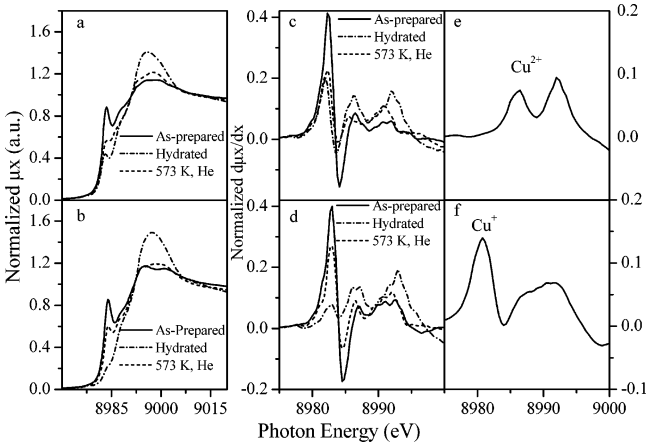

Figure 10. Cu K-edge XANES. Normalized absorption spectra of (a) Cu−USY and (b) Cu−ZSM-5. First derivative spectra of (c) Cu−USY and (d) Cu−ZSM-5 showing Cu^+ and Cu^{2+} inflection points. Standards for Cu^+ and Cu^{2+} are shown in (e) CuO and (f) Cu_2O with Cu^+ and Cu^{2+} features highlighted.

a part of the Cu^{2+} observed following hydration of both Cu−USY and Cu−ZSM-5 may be due to this process.

Since the majority of the Cu in as-prepared Cu−USY and Cu−ZSM-5 is present as Cu^+ in cation exchange positions, an effort was undertaken to determine the local environment of the Al and Cu cations associated with the exchange sites. Single scattering path simulations of $k^3\chi(k)$ were undertaken to identify the effects of Cu/Al ratio and R_{Al-Cu} on the peak observed in the region of 6−8 Å^{-1}, which is due in part to Al−Si, Al−O, and to Al−Cu backscattering. It is known from a study of the relative effective backscattering amplitudes (F_{eff}) that O < Si < Cu.[33b,d] Furthermore, a FEFF simulation shows that the effective backscattering amplitude for Al−Cu has its maximum contribution between 6 and 8 Å^{-1}. Multiscattering, which was not included in the simulation, has its main contribution at lower wavenumbers. The effect which Al−Cu scattering has on this part of the spectrum was evaluated by setting Al−O and Al−Si distances and varying Cu/Al ratio and R_{Al-Cu} systematically. Figure 12 shows the effects of both variables, as well as the experimentally observed scattering function for Cu−ZSM-5 and Cu−USY in vacuo at 298 K. It is evident that the appearance of the two peaks in the region of 6−8 Å^{-1} is a function of the Cu/Al ratio and that the relative height of the two peaks is a function of the magnitude of R_{Al-Cu}. The disagreement between the simulated and experimentally observed values of $k^3\chi(k)$ is due to the use of only single scattering paths in the simulation. Nevertheless, qualitative agreement between the simulated and experimentally observed peaks for the region of 6−8 Å^{-1} is obtained for Cu/Al = 1.00 and R_{Al-Cu} = 2.79 Å. The value of R_{Al-Cu} = 2.79 Å is comparable with those determined from quantum chemical simulations of Cu^+ exchange into the T12 site of ZSM-5 which range from, 2.76 Å to 2.80 Å[53,74,75] and Cu^+ exchanged into the site II position of Y zeolite, 2.94 Å.[76] The only previously reported value for Al−Cu separation in

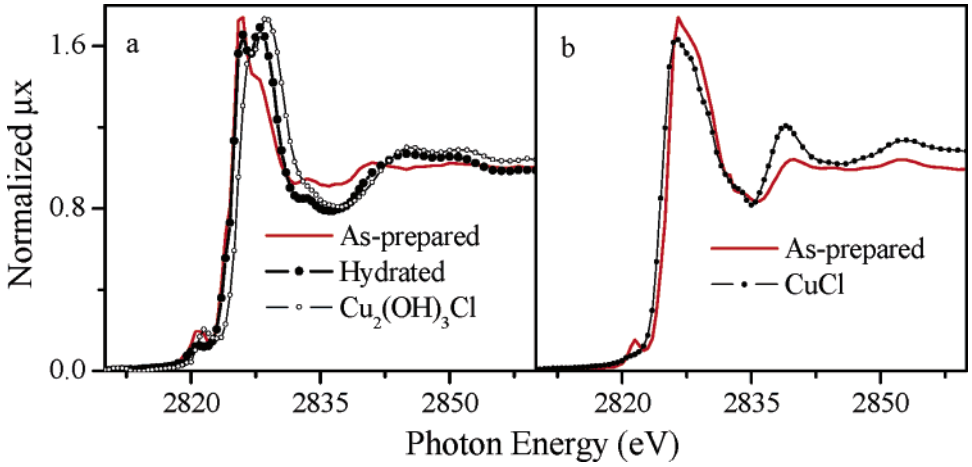

Figure 11. Cl K-edge XANES spectra of (a) Cu−USY and (b) Cu−ZSM-5.

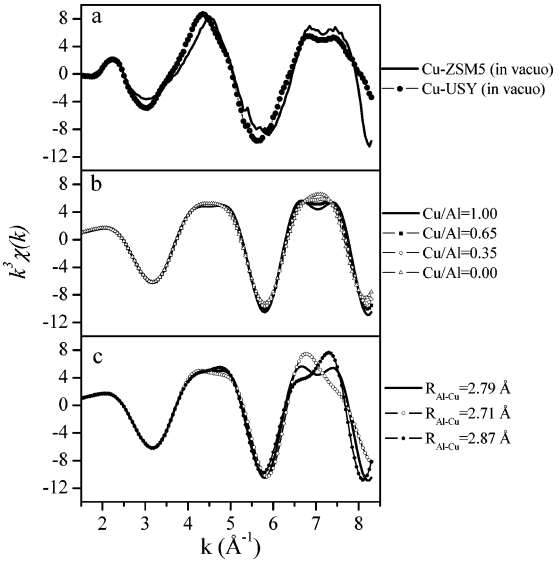

Figure 12. (a) $k^3\chi(k)$ of Cu−USY and Cu−ZSM-5 (both in vacuo). (b) Simulation of $k^3\chi(k)$ for different values of Cu/Al. Model parameters described in experimental section. (c) Simulation of $k^3\chi(k)$ for different values of R_{Cu-Al}. Model parameters are described in the Experimental Section.

Cu^+−ZSM-5 is 2.3 ± 2 Å, which was determined from ^{27}Al-^{65}Cu SEDOR NMR experiments.[77] The reason for the difference in the values of R_{Al-Cu} determined by Al K-edge EXAFS and NMR is not known.

Conclusion

In situ transmission Al K-edge EXAFS and XANES has been used to characterize the coordination of Al present in the framework of USY and ZSM-5 zeolites containing either NH_4^+, H^+, or Cu^+ as the charge-compensating cation. Al K-edge XANES of hydrated H−USY and H−ZSM-5 showed evidence for both tetrahedrally and octahedrally coordinated Al. Upon dehydration at elevated temperature, the octahedrally coordinated Al was converted progressively to tetrahedrally coordinated Al via the process described in Scheme 1. The quantity of water desorbed during the drying process is consistent with that indicated in the proposed mechanism. Much less octahedrally coordinated Al is present when either ammonium or cuprous cations act as the charge-compensating species. This is ascribed to the much lower affinity of these cations for water relative to protons. Analysis of Al K-edge EXAFS data indicates that the Al−O bond distance for tetrahedrally coordinated Al in dehydrated USY and ZSM-5 is 1.67 Å, a value about 0.05 Å shorter than the average value of this bond distance determined from DFT calculations. Simulation of $k3\chi(k)$ for Cu^+-exchanged ZSM-5 leads to an estimate of the distance between Cu and framework Al atoms. This distance is 2.79 Å, which is in close agreement with the distance determined from DFT studies of Cu-exchange ZSM-5.

Acknowledgment. This work was supported by the Director of the Office of Science, Office of Basic Energy Sciences, Division of Chemical Sciences, Geosciences, and Biosciences and the Division of Materials Sciences of the U.S. Department of Energy at the ALS and LBNL under Contract No. DE-AC02-05CH11231. Additional support was provided by the Methane Conversion Cooperative, funded by BP, and in part (TCNL) by the National Institutes of Health (HG01399).

References and Notes

(1) Breck, D. W. *Zeolite Molecular Sieves: Structure, Chemistry and Use*; Krieger: Melbourne, 1984.

(2) Van Bekkum, H.; Flanigen, E. M.; Jacobs, P. A.; Jansen, J. C.; Eds. *Introduction to Zeolite Science and Practice*, 2nd ed.; Elsevier: Amsterdam, 2001.

(3) Weitkempt, J.; Ernst, S.; Daums, H.; Gallie, E. *Chem. Eng. Technol.* **1986**, *58*, 623.

(4) Stocker, M. *Microporous Mesoporous Mater.* **1999**, *29*, 3.

(5) Weitkempt, J.; Puppe, L. *Catalysis and Zeolites, Fundamentals and Applications*; Springer-Verlag: Berlin, 1999.

(6) (a) Kramer, G. J.; van Santen, R. A. *J. Am. Chem. Soc.* **1993**, *115*, 2887. (b) van Santen, R. A.; Kramer, G. J. *J. Chem. Rev.* **1995**, *95*, 637.

(7) Eichler, U.; Brändle, M.; Sauer, J. *J. Phys. Chem. B* **1997**, *101*, 10035.

(8) Campana, L.; Selloni, A.; Weber, J.; Goursot, A. *J. Phys. Chem. B* **1997**, *101*, 9932.

(9) (a) Berthomieu, D.; Ducéré, J. M.; Goursot, A. *J. Phys. Chem. B* **2002**, *106*, 7483.

(10) (a) Wilson, A. J. C. *International tables for X-ray crystallography, vol C, Mathemathical, physical and chemical tables*; Kluwer Academic Publishers: Dordrecht, 1992. (b) Cheetham, A. K.; Thomas, J. T.; Eddy, M. M.; Jefferson, D. A. *Nature* **1982**, *299*, 24.

(11) Klinowski, J.; Fyfe, C. A.; Gobbi, G. C. *J. Chem. Soc., Faraday Trans. 1* **1985**, *81*, 3003.

(12) Freude, D.; Brunner, E.; Pfeifer, H.; Prager, D.; Jerschkewitz, H. G.; Lohse, U.; Oehlmann, G. *Chem. Phys. Lett.* **1987**, *139*, 325.

(13) Shertukde, P. V.; Hall, W. K.; Dereppe, J. M.; Marcelin, G. *J. Catal.* **1993**, *139*, 468.

(14) Grober, P. J.; Geerts, H.; Tielen, M.; Martens, J. A.; Jacobs, P. A. *Stud. Surf. Sci. Catal.* **1989**, *46*, 721.

(15) Frydman, L.; Harwood, J. S. *J. Am. Chem. Soc.* **1995**, *117*, 5367.

(16) (a) Fyfe, C. A.; Bretherton, J. L.; Lam, L. Y. *Chem. Commun.* **2000**, 1575. (b) Fyfe, C. A.; Bretherton, J. L.; Lam, L. Y. *J. Am. Chem. Soc.* **2001**, *123*, 5285.

(17) Omegna, A.; van Bokhoven, J. A.; Prins, R. *J. Phys. Chem. B* **2003**, *107*, 8854.

(18) Bourgeat-Lami, E.; Massiani, P.; Di Renzp, F.; Espiau, P. Fajula, F. *Appl. Catal.* **1991**, *72*, 139.
(19) Wouters, B. H.; Chen, T. H.; Grobet, P. J. *J. Am. Chem. Soc.* **1998**, *120*, 11419.
(20) (a) Kentgens, A. P. M.; Iuga, D.; Kalwei, M.; Koller, H. *J. Am. Chem. Soc.* **2001**, *123*, 2925. (b) Kanellopoulos, J. J.; Wang, J. W.; Ray, S. S.; Foerster, H.; Freude, D.; Hunger; M. *Phys. Chem. Chem. Phys*. **2005**, *17*, 3221.
(21) Petunchi, J. O.; Marcelin, G.; Hall, W. K. *J. Phys. Chem.* **1992**, *96*, 9967.
(22) Corbin, D. R.; Burgess, B. F., Jr.; Vega, A. J.; Farlee, R. D. *Anal. Chem.* **1987**, *59*, 2722.
(23) van Bokhoven, J. A.; van der Eerden A. M. J.; Koningsberger, D. C. *Stud. Surf. Sci. Catal.* **2002**, *142*, 1885.
(24) van Bokhoven, J. A.; Koningsberger, D. C.; Kunkeler, P.; van Bekkum, H. *J. Catal.* **2002**, *211*, 540.
(25) Joyner, R. W.; Smith, A. D.; Stockenhuber, M.; van der Berg, M. W. E. *Phys. Chem. Chem. Phys.* **2004**, *6*, 5435.
(26) Bugaev, L. A.; van Bokhoven, J. A.; Sokolenko, A. P.; Latokha, Y. V.; Avakyan, L. A. *J. Phys. Chem. B* **2005**, *109*, 10771.
(27) Omegna, A.; Prins, R.; van Bokhoven, J. A. *J. Phys. Chem. B* **2005**, *109*, 9280.
(28) Drake, I.; Liu, C. N.; Gilles, M.; Tyliszczak, T.; Kilcoyne, A. L. D.; Shuh, D.; Mathies, R. A.; Bell, A. T. *Rev. Sci. Instrum.* **2004**, *75*, 3242.
(29) Underwood, J. H.; Gullikson, E. M. *J. Electron Spectrosc. Relat. Phenom.* **1998**, *92*, 265.
(30) Nachimuthu, P.; Matsuo, S.; Farangis, B.; Lindle, D. W.; Wakita, H.; Perera, R. C. C. *J. Alloys Compd.* **2004**, *362*, 124.
(31) ALS internal communication: http://www-als.lbl.gov/als/compendium. Matsuo, S.; Kurisaki, T.; Yamashige, H.; Nachimuthu, P.; Perera, R. C. C.; Wakita, H. Development and evaluation of a new liquid cell system for soft X-ray absorption experiments.
(32) Values were calculated using the web interface of the Center for X-ray Optics at Lawrence Berkeley National Laboratory, Berkeley, CA: http://www-cxro.lbl.gov/optical_constants/pert_form.html.
(33) (a) Stern, E. A.; Kim, K. *Phys. Rev. B* **1981**, *23*, 378. (b) Koningsberger, D. C.; Prins, R. *X-ray Absorption*; Wiley: New York, 1988. (c) Koningsberger, D. C.; Mojet, B. L.; van Dorssen, G. E.; Ramaker, D. E. *Top. Catal.* **2000**, *10*, 143. (d) Teo, B. K. *EXAFS: Basic Principles and Data-analysis*; Springer: New York, 1986.
(34) Kilcoyne, A. L. D.; Tyliszczak, T.; Steele, W. F.; Fakra, S.; Hitchcock, P.; Franck, K.; Anderson, E.; Harteneck, B.; Rightor, E. G.; Mitchell, G. E.; Hitchcock, A. P.; Yang, L.; Warwick T.; Ade, H. *J. Synchrotron Rad.* **2003**, *10*, 125.
(35) Stern, E. A.; Newville, M.; Ravel, B.; Yacoby, Y.; Haskel, D. *Physica B* **1995**, *208*−*209*, 117.
(36) Shadle, S. E.; Hedman, B.; Hodgson, K. O.; Solomon, E. I. *Inorg. Chem.* **1994**, *33*, 4235.
(37) Hedman, B.; Hodgson, K. O.; Solomon, E. I. *J. Am. Chem. Soc.* **1990**, *112*, 1543.
(38) Hedman, B.; Frank, P.; Gheller, S. F.; Roe, A. L.; Newton, W. E.; Hodgson, K. O. *J. Am. Chem. Soc.* **1988**, *110*, 3798.
(39) Drake, I. J.; Fujdala, K. L.; Bell, A. T.; Tilley, T. D. *J. Catal.* **2005**, *230*, 14.
(40) Jentoft, R. E.; Deutsch, S. E.; Gates, B. C. *Rev. Sci. Instrum.* **1996**, *67*, 2111.
(41) Drake, I. J.; Fujdala, K. L.; Baxamusa, S.; Bell, A. T.; Tilley, T. D. *J. Phys. Chem. B* **2004**, *108*, 18421.
(42) Stern, E. A.; Newville, M.; Ravel, B.; Yacoby, Y.; Haskel, D. *Physica B* **1995**, *208*−*209*, 117.
(43) (a) Newville, M. *J. Synchrotron Radiat.* **2001**, *8*, 322. (b) IFEFFIT manual: http://cars9.uchicago.edu/ifeffit/ (c) Ravel, B.; Newville, M. *Phys. Scr.* **2005**, *T115*, 1007.
(44) Newville, M.; Lĭviņš, P.; Yacoby, Y.; Rehr, J. J.; Stern, E. A. *Phys. Rev. B* **1993**, *47*, 14126.
(45) Ankudinov, A. L.; Rehr, J. J. *Phys. Rev. B* **1997**, *56*, R1712.
(46) Ankudinov, A. L.; Bouldin, C.; Rehr, J. J.; Sims, J.; Hung, H. *Phys. Rev. B* **2002**, *65*, 104107.
(47) (a) Poiarkova, A. V.; Rehr, J. J. *Phys. Rev. B* **1999**, *59*, 948. (b) Rehr, J. J.; Albers, R. C. *Rev. Mod. Phys.* **2000**, *72*, 621.
(48) Killean, R. C. G. *J. Phys. F: Metal Phys.* **1974**, *4*, 1908.
(49) O'Day, P. A.; Rehr, J. J.; Zabinsky, S. I.; Brown, G. E., Jr. *J. Am. Chem. Soc.* **1994**, *116*, 2938.
(50) This statistical value is related to the standard definition of χ^2 but is normalized to the number of degrees of freedom in the fit. The details of this calculation have been described elsewhere. Newville, M.; Ravel, B.; Haskel, D.; Rehr, J. J.; Stern, E. A.; Yacoby, Y. *Physica B* **1995**, *208*−*209*, 154.
(51) Wachtman, J. B., Jr.; Tefft, W. E.; Lam, D. G., Jr.; Apstein, C. S. *Phys. Rev.* **1961**, *122*, 1754.
(52) Poiarkova, A. V.; Rehr, J. J. *Phys. Rev. B* **1999**, *59*, 948.
(53) Rice, M. J.; Chakraborty, A. K.; Bell, A. T. *J. Phys. Chem. A* **1998**, *102*, 7498.
(54) Joly, J. F.; Zanier-Szyldowski, N.; Colin, S.; Raatz, F.; Saussey, J.; Lavalley, J. C. *Catal. Today* **1991**, *9*, 31.
(55) (a) Datka, J.; Geerlings, P.; Mortier, W.; Jacobs, P. *J. Phys. Chem.* **1985**, *89*, 3483. (b) Flanigen, E. M. In *Zeolite Chemistry and Catalysis*; Rabo, J. A., Ed.; American Chemical Society: Washington, DC, 1976; ACS Monograph No. 171, p 93.
(56) Loeffler, E.; Lohse, U.; Peuker, C.; Oehlmann, G.; Kustov, L. M.; Zholobenko, V. L.; Kazansky, V. B. *Zeolites* **1990**, *10*, 267.
(57) (a) Jacobs, P. A.; Uytterhoeven, J. B. *J. Chem. Soc., Faraday Trans. 1* **1973**, *2*, 373. (b) Fritz, P. O.; Lunsford, J. H. *J. Catal.* **1989**, *118*, 85.
(58) Dias, S. C. L.; de Macedo J. L.; Dias, J. A. *Phys. Chem. Chem. Phys.* **2003**, *5*, 5575.
(59) (a) Meadows, M. D.; Smith, K. A.; Kinsey, R. A.; Rothgeb, T. M.; Skarjune, R. P.; Oldfield, E. *Proc. Natl. Acad. Sci. U.S.A.* **1982**, *79*, 1351. (b) Mastikhin, V. M.; Krivoruchko, O. P.; Zolotovskii, B. P.; Bayanov, R. A. *React. Kinet. Catal. Lett.* **1981**, *18*, 117. (c) Fyfe, C. A.; Gobbi, C. G.; Hartman, J. S.; Klinowski, J.; Thomas, J. M. *J. Phys. Chem.* **1982**, *86*, 1247.
(60) Klinowski, J.; Thomas, J. M.; Fyfe, C. A.; Gobbi, G. C. *Nature* **1982**, *296*, 533.
(61) Bourgeat-Lami, E.; Massiani, P.; Di Renzp, F.; Espiau, P. Fajula, F. *Appl. Catal.* **1991**, *72*, 139.
(62) van Bokhoven, J. A.; Sambe, H.; Ramaker, D. E.; Koningsberger, D. C. *J. Phys. Chem. B* **1999**, *103*, 7557.
(63) Shimizu, K.; Kato, K.; Yoshida, T.; Yoshida, H.; Satsuma, A.; Hattori, T. *Chem. Commun.* **1999**, 1681.
(64) McKeown, D. A.; Waychunas, G. A.; Brown, G. E., Jr. *J. Non-Cryst. Solids* **1985**, *74*, 349.
(65) Cabaret, D.; Sanictavit, P.; Ildefonse, P. Flank, A. M. *J. Phys.: Condens. Matter* **1996**, *8*, 3691.
(66) Ramachandran, C. E.; Williams, B. A.; van Bokhoven, J. A.; Miller, J. T. *J. Catal.* **2005**, *233*, 100.
(67) van Bokhoven, J. A.; van der Eerden, A. M. J.; Prins, R. *J. Am. Chem. Soc.* **2004**, *126*, 4506.
(68) Jungsuttiwong, S.; Limtrakul, J.; Truong, T. N. *J. Phys. Chem. B* **2005**, *109*, 13342.
(69) Zygmunt, S. A.; Curtiss, L. A.; Iton, L. E. *J. Phys. Chem. B* **2001**, *105*, 3034.
(70) Limtrakul, J.; Chuichay, P.; Nokbim, S. *J. Mol. Struct.* **2001**, *560*, 169.
(71) Ehresmann, J. O.; Wang, W.; Herreros, B.; Luigi, D. P.; Venkatraman, T. N.; Song, W.; Nicholas, J. B.; Haw, J. F. *J. Am. Chem. Soc.* **2002**, *124*, 10868.
(72) Yuan, S. P.; Wang, J. G.; Li, Y. W.; Jiao, H. *J. Phys. Chem. A* **2002**, *106*, 8167.
(73) (a) Tennent, N. H.; Antonio, K. M. Bronze disease: Synthesis and characterisation of botallackite, paratacamite and atacamite by infrared spectroscopy. *ICOM Committee for Conservation preprints*, 6th Triennial Meeting, Ottawa, 1981. (b) Sharkey, J. B.; Lewin, S. Z. *Am. Min.* **1971**, *56*, 179.
(74) Treesukol, P.; Limtrakul, J.; Truong, T. N. *J. Phys. Chem. B* **2001**, *105*, 2421.
(75) Rodriquez-Santiago, L.; Sierka, M.; Branchadell, V.; Sodupe, M.; Sauer, J. *J. Am. Chem. Soc.* **1998**, *120*, 1545
(76) Berthomieu, D.; Krishnamurty, S.; Coq, B.; Delahay, G.; Goursot, A. *J. Phys. Chem. B* **2001**, *105*, 1149.
(77) Hu, S.; Reimer, J. A.; Bell, A. T. *J. Phys. Chem. B* **1997**, *101*, 1869.